Acta Acustica 2026, **10**, 39

https://doi.org/10.1051/aacus/2026036

Available online at:
https://acta-acustica.edpsciences.org

New Approaches and Perspectives in Building Acoustics

Scientific Article Open Access

Finite element modelling of bracket-connected cross-laminated timber plates to calculate vibration reduction indices

Antonio Esposito[1,*], Sven Vallely[2], Blaž Kurent[3], and Stefan Schoenwald[1]

[1]Swiss Federal Laboratories for Materials Science and Technology (Empa), Überlandstrasse 129, 8600 Dübendorf, Switzerland
[2]KU Leuven, Dept. of Civil Engineering, Kasteelpark Arenberg 40, 3001 Leuven, Belgium
[3]University of Ljubljana, Faculty of Civil and Geodetic Engineering, Jamova cesta 2, 1000 Ljubljana, Slovenia

Received 15 January 2026, Accepted 4 April 2026

Abstract – Several modelling approaches have been developed to predict flanking sound transmission through Cross-Laminated Timber (CLT) junctions, typically assuming idealised connections. However, research has shown that the configuration of fasteners significantly influences flanking sound transmission in these junctions. Predicting such effects requires versatile models where connectors are modelled accurately. This paper presents an experimentally validated Finite Element Method (FEM) model of an L-junction mock-up, where the angle brackets connecting CLT plates are represented in detail. As part of the validation, the Vibration Reduction Index K_{ij} is reported for two different configurations of the L-junction, with plates being either in direct contact or separated by an air gap. The mechanical contact at plates' interface has been modelled accordingly with coupling stiffness matrices. Numerical results showed a good correlation to experimental data in one-third octave bands, with deviations of less than 5 dB up to 3150 Hz. Analysis identified that: (1) an interrelationship exists between connectors and contact mechanics at the plates' interface; (2) connectors can be modelled using this methodology, although they cannot be reduced to mere rigid point connections; (3) modelling connectors in detail is necessary for accurate predictions, especially when the plates' contact interface is far from rigid.

Keywords. Cross-Laminated Timber (CLT), Vibration Reduction Index (K_{ij}), Finite Element Method (FEM)

1 Introduction

In recent years, Cross-Laminated Timber (CLT) has become a well-established building element in the construction sector owing to its validated performance in structural applications, inherent fire resistance characteristics, cost optimization potential, and its contribution to sustainable building practices [1, 2]. Due to the engineered lay-up, CLT has a reduced orthotropy in comparison to alternative wood materials. Moreover, compared to concrete and masonry, CLT has a generally higher strength-to-weight ratio, which results in the use of lighter building elements. While lightweight construction offers many benefits, it is also causing non-optimal sound insulation performance of building partitions and, in particular, significant structure-borne sound power flow across their junctions [3]. The distinguishing features of CLT connections can be categorised into two main types: floor-to-floor joints and wall-to-floor connections. For the former case, a non-exhaustive list of examples includes glued joints [4], splines and half-lapped or butt joints [5]. Wall-to-floor building connections, which constitute the primary focus of this study, are usually assembled with the use of crossing screws, screwed or nailed metal brackets and hold-downs, especially for specific types such as L-, T- or X- junctions [6, 7]. Given the above, alongside the significant advancements made in the field of material characterisation [8, 9], the numerical modelling of flanking sound transmission mechanisms in CLT junctions has received special attention in scientific research, with a view to predicting the Vibration Reduction Index K_{ij}, as defined by the ISO 12354-1:2017 standard [10]. This is an important quantity in analysing flanking sound transmission in CLT buildings. For this purpose, part of the outcomes of the research project "Schallschutz im Holzbau", conducted in cooperation by Empa and Lignum, the umbrella organisation of the Swiss forestry and timber industry, are presented in this paper.

Since the connection of CLT plates is typically accomplished through the utilisation of point connectors in conjunction with the direct mechanical contact between CLT

*Corresponding author: antonio.esposito@empa.ch

elements [6], it is often particularly challenging to provide an accurate estimation of the K_{ij} index. Therefore, separately modelling the contact mechanisms at the plate-plate and plate-connector interfaces may contribute to build up versatile Finite Element Method (FEM) models, which include a detailed representation of connectors. Potentially, this may allow to bypass the need of updating numerical models with experimental data, which generally require to set up expensive test-rigs for each particular case.

In acoustics, the existing approaches for K_{ij} prediction rely either on empirical or analytical models. In particular, the ISO 12354-1:2017 standard [10] provides empirical formulae, based on few laboratory measurements, to compute K_{ij} for T- and X- CLT junctions [10, 11]. Nevertheless, such relationships are considered valid only for junctions between elements with a mass per unit area ratio between 0.5 and 2. Moreover, a marked discrepancy between predicted and measured data is reported in [6, 12], where it is also demonstrated that K_{ij} can be significantly influenced based on the type of connectors utilised in the tested junction. This highlights the necessity to expand the scope of applicability of this model.

Alongside empirical formulae, analytical models have been introduced for modelling connections between CLT plates. These are based on fundamental assumptions, such as semi-infinite plates and the simplification of contact interfaces by means of ideal line connections. Although this makes such models cost-effective, it also makes challenging to predict the effects of differences in connector type. For example, in [13], a computationally efficient analytical wave approach has been proposed, relying on the framework by Langley and Heron [14], with the aim of predicting the Vibration Reduction Index K_{ij} through CLT plates in the presence of resilient interlayers. This model was validated for CLT junctions with and without resilient strips, which were represented using three different material models. Results in terms of K_{ij} have shown different degrees of accuracy depending either on the rigid or elastic behaviour of the plates' connection. For junctions with resilient interlayers, the most accurate results showed deviations below 5 dB in most of the one third-octave bands. In the case of X-junctions without interlayers, the accuracy of K_{ij} predictions was strongly dependent on the degree of rigidity of the analysed fasteners, due to the assumption of infinitely rigid line connection. For the stiffer paths of a screwed junction, the deviation from experimental data laid below 5 dB in the majority of one third-octave bands, but reached values up to 12 dB for paths with less rigid connections. This shows that estimating the influence of connectors in K_{ij} predictions still constitutes a challenging task.

The relevant effects exerted by connectors on flanking sound transmission in CLT junctions have been also demonstrated in the context of a previous research conducted at Empa. In particular, an experimental parametric study was conducted to investigate flanking sound transmission across the junction of a mass timber floor with an exterior wall, with and without elastic interlayers and using rigid or decoupled steel angle brackets [15]. In one of the specimen combinations, the K_{ij} of a T-junction with a resilient interlayer was measured once using rigid angle brackets and once decoupling them from the plates by means of an elastic layer. Experimental data showed a 6.7 dB difference between the K_{ij} of the two configurations, averaged over the frequency range from 200 Hz to 1.25 kHz. Analogous effects are highlighted in [6], where it is found that K_{ij} in CLT wall-to-floor junctions can vary depending on the fastening configuration. These findings further substantiate the necessity of employing a detailed modelling approach in the analysis of connectors.

The detailed FEM modelling of CLT plate connectors (in particular, angle brackets and hold-downs) is a common approach in the field of structural engineering. In most cases, it is adopted for seismic design purposes, with the aim of investigating the mechanical behaviour of connectors when approaching failure conditions. To predict such mechanisms in CLT wall-to-floor connections, Izzi et al. [16] performed non-linear FEM simulations on typical CLT junctions, connected with hold-downs or angle brackets. In particular, the latter were modelled as three-dimensional solid bodies, and the nailed joints simulated as non-linear hysteretic springs. Numerical shear and tension tests, carried out in monotonic and cyclic conditions, showed low deviations against the data obtained from experimental tests conducted on similar junctions. On this basis, it is therefore reasonable to propose that such FEM analyses could be used as a preliminary reference point for detailed modelling of connectors also in the domain of linear dynamics.

In structural dynamics analyses at a building scale, CLT connections have been modelled in FEM with reduced-order approaches also being used [17, 18]. These contributions demonstrate the applicability of FEM at a larger scale, underscoring the robustness of reduced-order representation of connections. Nevertheless, in order for these approaches to be effective for acoustic analyses, a detailed preliminary characterisation of connectors is necessary.

The reliability of FEM-based approaches to accurately predict vibration transmission is also addressed in [19–21], where FEM results were utilised as a numerical reference for validation of Statistical Energy Analysis (SEA) and wave theory algorithms, in the case of heavyweight walls and floors junctions.

Building upon the preliminary findings outlined in [22], a FEM model is presented hereby, which introduces specific elements for the prediction of structure-borne flanking sound transmission in mass timber buildings: the detailed representation of connectors, the simplification of the mechanical contact between plates with linear springs and the extension of FEM simulations to a broader frequency range. Based on the above, an alternative approach is hereby put forward as a potential initial phase in a top-down procedure for constructing versatile FEM models, starting from the dynamic characterisation of junction components. In particular, the sample

under examination is a CLT L-junction mock-up, where each component is modelled independently and subsequently assembled for the purpose of conducting modal and harmonic response analyses. As a preliminary step, the geometry of a steel angle bracket is modelled in detail and validated against laser vibrometry measurements. Two CLT plates are then modelled and connected with two of the aforementioned brackets, with a specific focus on the definition of strategies for modelling the fastening systems and the mechanical contact between CLT plates. This makes it possible to analyse the mechanical behaviour of the system in different configurations, where the plates are either in direct contact with each other or mechanically decoupled by an air gap. This way, the influence of both connectors and mechanical contact between plates on the structure-borne flanking transmission in the L-junction can be numerically and experimentally investigated. Limitations and possible applicability of such methodology are then explored by means of further numerical analyses, where simplifications of the model are proposed and compared to the original version.

The structure of the paper is as follows: in Section 2, the theory underlying the FEM analyses is outlined together with the framework for the measurement of the K_{ij} index, according to the ISO 10848-1:2017 and the ISO 10848-4:2017 standards [23, 24]. In Section 3, the modelling methodology is presented, with a comprehensive description of the sample, a detailed exposition of the modelling approach for each individual component of the junction and their preliminary validation against experimental measurements in the modal domain. In Section 4, the validation of the L-junction model is presented both in the low and high modal density regions. Numerical results are compared in terms of eigenfrequencies, mode shapes and K_{ij} against the experimental data obtained from different configurations of the L-junction. In Section 5, results are discussed and further analysed to investigate the importance of modelling connectors in relation to their effects on the mechanical behaviour of the system. In Section 6, conclusions and possible future developments are outlined.

2 Background and theory

In this section, the theoretical background underlying the numerical and experimental analyses carried out on the proposed model is described. FEM modal analyses were conducted both on the decoupled components of the L-junction, i.e. plates and angle brackets, which were modelled independently, and on the model of the assembled L-junction. The results of these simulations were validated against experimental data in the low modal density domain. FEM harmonic response analyses were performed only on the assembled L-junction model. The dynamic response of the system, in terms of transverse velocity, served as a basis to calculate the Vibration Reduction Index (K_{ij}). The theory underpinning these analyses is described in Section 2.1. To validate the model in the high modal density region, the K_{ij} index was also determined experimentally and the framework for the measurement is described in Section 2.2 according to the guidelines provided in the ISO 10848-1:2017 standard [23]. It should be noted that the K_{ij} index is referred to in this paper solely for the purpose of experimentally validating the proposed FEM modelling methodology, and not for providing general predictions in the field of building design. For this reason, and due to the reduced dimensions of the scaled sample, not all the requirements for the standardised K_{ij} measurement procedure are met. Moreover, given the application of this approach to both measured and simulated data, it is reasonable to assume that the same uncertainties apply to both sets of data. Deviations from the standardised measurement requirements are acknowledged in detail in Section 4.1. In Section 2.3, the metrics used to validate the proposed numerical models in the low modal density region are defined.

2.1 Modal and harmonic analyses in FEM

The equation of motion of an undamped multi-degree of freedom (MDOF) system in free vibration conditions can be written as [25, 26]:

$$[\mathbf{M}]\{\ddot{\mathbf{u}}\} + [\mathbf{K}]\{\mathbf{u}\} = \{\mathbf{0}\} \tag{1}$$

where $\{\ddot{\mathbf{u}}\} \in \mathbb{C}^n$ is the nodal acceleration vector, $\{\mathbf{u}\} \in \mathbb{C}^n$ is the nodal displacement vector, $[\mathbf{M}] \in \mathbb{R}^{n\times n}$ is the mass matrix, $[\mathbf{K}] \in \mathbb{R}^{n\times n}$ is the stiffness matrix of the system and $n \in \mathbb{R}$ is the number of degrees of freedom of the FEM model.

For linear systems, the displacement field solutions of equation (1) are harmonic of the form:

$$\{\mathbf{u_i}\} = \{\boldsymbol{\phi_i}\}\cos(\omega_i t) \tag{2}$$

where the ith natural circular frequency ω_i and the eigenvector $\boldsymbol{\phi_i}$ of the system can be calculated by solving the following eigenvalue problem:

$$([\mathbf{K}] - \omega_i^2[\mathbf{M}])\{\boldsymbol{\phi_i}\} = \{\mathbf{0}\}. \tag{3}$$

When the system is excited by an external harmonic force $\{\mathbf{F}\}$ and hysteretic damping is included, equation (1) becomes [26]:

$$[\mathbf{M}]\{\ddot{\mathbf{u}}\} + [\mathbf{K} + \mathbf{iH}]\{\mathbf{u}\} = \{\mathbf{F}\} \tag{4}$$

where $\{\mathbf{F}\} \in \mathbb{C}^n$ is the external harmonic forcing vector and $[\mathbf{H}]$ is the structural damping matrix of the system. For the purpose of the simulations presented herein, material-dependent constant structural damping coefficients η_j have been defined for each jth body of the system. The use of such damping coefficients facilitates the inclusion of hysteretic behaviour, attributable to internal material friction, through the specification of a coefficient within the stiffness matrix. To solve the harmonic response analyses, the full solution method was adopted, which solves equation (4) directly [26].

2.2 Vibration Reduction Index (K_{ij})

In order to predict the flanking sound transmission across a junction between building elements, the ISO 12354-1:2017 and the ISO 10848-1:2017 standards [10, 23] introduce the Vibration Reduction Index K_{ij}. This frequency-dependent quantity, expressed in decibels, is based on Statistical Energy Analysis (SEA) assumptions on vibration energy transmission. It can be written as:

$$K_{ij} = \overline{D_{v,ij}} + 10lg\left(\frac{l_{ij}}{\sqrt{a_i a_j}}\right). \tag{5}$$

This quantity represents the direction-averaged velocity level difference $\overline{D_{v,ij}}$ between two elements, normalized to the junction length l_{ij} and the equivalent absorption lengths $a_{i,j}$ of the elements i and j. These are defined as [23]:

$$a_{i,j} = \frac{2.2\pi^2 S_{i,j}}{c_0 T_{s,i,j}}\sqrt{\frac{f_{\text{ref}}}{f}} \tag{6}$$

where $S_{i,j}$ and $T_{s,i,j}$ are respectively the surface area and the structural reverberation time of the elements i or j, c_0 is the speed of sound in air, f is the centre band frequency of analysis and f_{ref}, equal to 1000 Hz, is the reference frequency.

According to [23], CLT panels can be classified as Type A elements, since their behavior can be significantly influenced by the boundary conditions. For this reason, the modal overlap factor M becomes important to define the lower frequency limit for the K_{ij} measurement to be considered reliable. It is defined as [24]:

$$M = \frac{2.2n}{T_{s,i,j}} \tag{7}$$

where n is the modal density, measured in modes per hertz. The modal overlap factor describes how much two neighbouring modal peaks are overlapping. If $M > 1$ the half power bandwidth of the modes overlap. A minimum value of $M = 1$ ensures that uncertainties remain within an acceptable range for reliable prediction of K_{ij}.

2.3 Validation metrics

Based on [9], the validation of the proposed FEM models in the low modal density region is achieved referring to two specific metrics, calculated from the comparison against experimental data. Firstly, the absolute value of the relative difference between numerical and experimental eigenfrequencies, expressed in percentage, is quantified by means of the Percentage Error index (PE), defined as:

$$PE(f_k^{fe}, f_l^{ex}) = \left|\frac{f_k^{fe} - f_l^{ex}}{f_l^{ex}}\right| \times 100\% \tag{8}$$

where:

- f_k^{fe} are the $k \in \mathbb{N}$ eigenfrequencies of the numerical solution;
- f_l^{ex} are the $l \in \mathbb{N}$ eigenfrequencies of the experimental solution.

According to what is defined in [9], a PE $< 10\%$ is set as an acceptability criterion for validation.

The degree of correlation between numerical and experimental mode shapes is quantified by the Modal Assurance Criterion (MAC). This index is a squared linear regression correlation coefficient between numerical and experimental eigenvectors, defined as [27]:

$$\text{MAC}(\phi_k^{fe}, \phi_l^{ex}) = \frac{\left|(\phi_k^{fe^T} \cdot \phi_l^{ex})\right|^2}{\left|\phi_k^{fe^T} \cdot \phi_k^{fe}\right| \cdot \left|\phi_l^{ex^T} \cdot \phi_l^{ex}\right|} \tag{9}$$

where:

- $\phi_k^{fe} \in \mathbb{C}^n$ are the $n \in \mathbb{N}$ degree of freedom mode shapes of the numerical solution;
- $\phi_l^{ex} \in \mathbb{C}^n$ are the $n \in \mathbb{N}$ degree of freedom mode shapes of the experimental solution.

The index in question is defined within the interval from 0 to 1, with 1 denoting an exact correlation and 0 denoting no correlation between the two sets of data.

3 FEM modelling methodology of a CLT L-junction

In this section, the main steps of the FEM methodology adopted in this study are reported in detail. A description of the geometrical features of the analysed L-junction mock-up is provided in Section 3.1. This is followed, in Sections 3.2 and 3.3, by the numerical characterisation of the elements constituting the system, namely the CLT plates and the steel angle brackets. The validation process of these FEM models is described, by comparing the numerical results in the low modal density region to the experimental data obtained from vibrometry measurements performed on standalone brackets and plates. A particular focus has been placed on the modelling strategies adopted to define the plate-to-plate and bracket-to-plate contact interfaces, outlined in Section 3.4. In Section 3.5, a description of the FEM model and the numerical analyses carried out on the assembled L-junction system is provided in detail.

3.1 Description of the L-junction mock-up

The FEM methodology presented in this paper applies to the CLT L-junction mock-up illustrated in Figures 1 and 2. Two CLT plates of different dimensions and lay-up (henceforth referred to as CLT100 and CLT060) are connected by means of two steel angle brackets so that one plate is positioned perpendicular along one edge of the other (Fig. 1a). A detailed description about the lay-up structure and the mechanical properties of the individual plates is provided in Section 3.2. Different experimental configurations of the mock-up were tested. These are defined as follows:

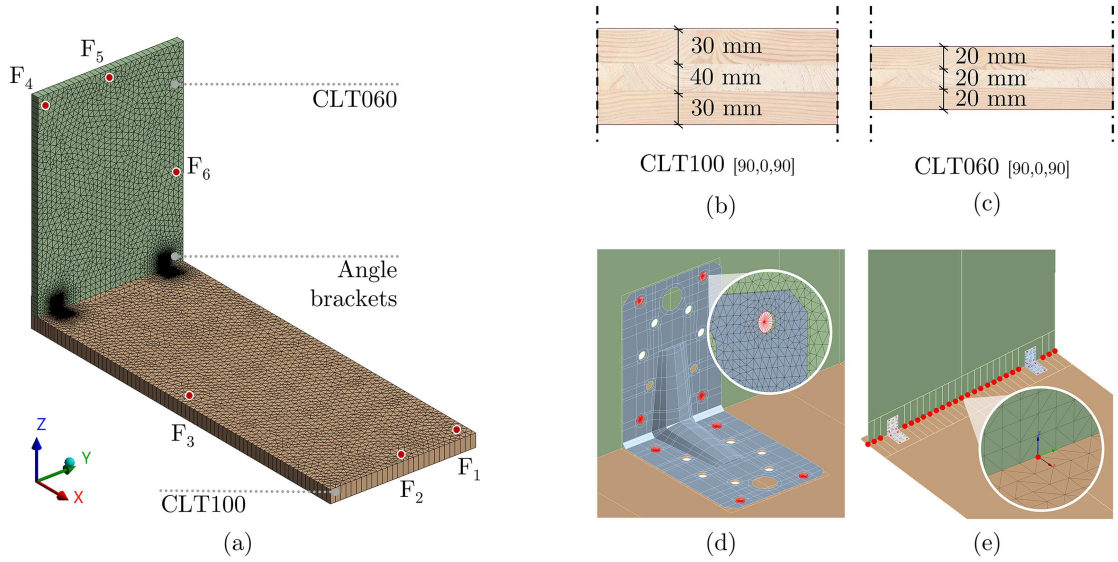

Figure 1. FEM model of the L-junction mock-up: (a) discretisation of the assembled mock-up. The red circular markers represent the excitation positions F_1 to F_6 for harmonic analyses. (b), (c) Lay-ups of the CLT100 and CLT060 plates. (d) Detailed model of the bracket with a close-up of the fastening points, whereby rigid multi-point constraints are applied at the plate-bracket interface along the screw holes highlighted in red. (e) Schematisation of the nodal coupling stiffness joints (red dots) applied at the plate-plate interface.

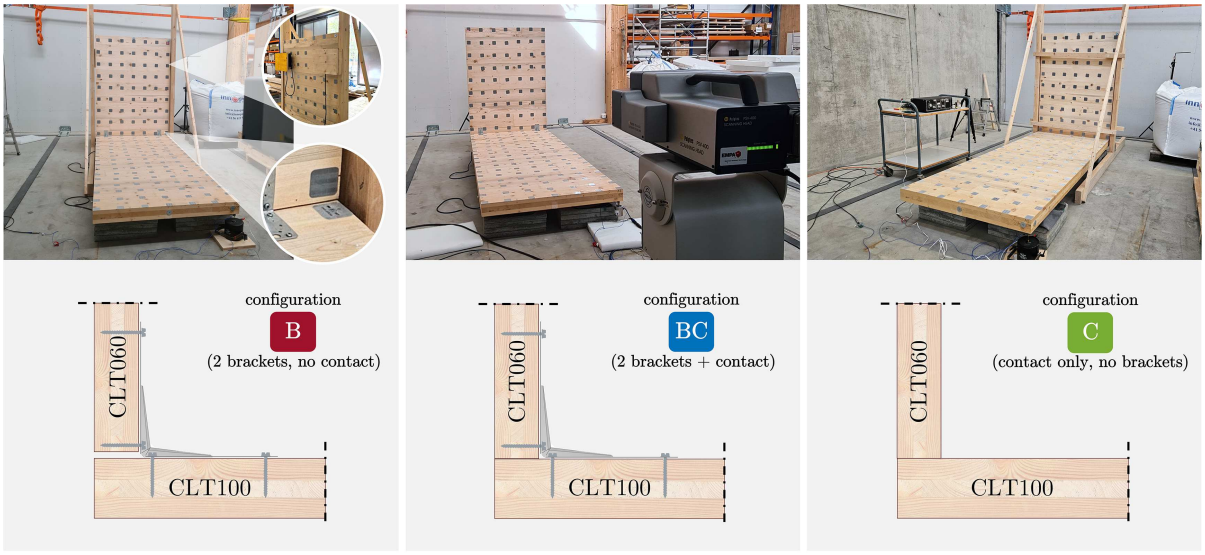

Figure 2. Experimental set-up of the L-junction mock-up. Top: (a) photo of configuration B, with close-ups on the gap between plates and the safety frame; (b) photo of configuration BC; (c) photo of configuration C. Bottom: schematisation of the fastening systems and plates' contact interface of configurations (a) B, (b) BC and (c) C.

– **B**, where 'B' stands for 'brackets'. In this configuration, two angle brackets are used to connect the CLT plates. Direct mechanical contact between plates is prevented by a 3 mm air gap at the plate-plate interface (Fig. 2a). The objective of this configuration is to ascertain the contribution of energy transmission attributable exclusively to the brackets;
– **BC**, where 'B' stands for 'brackets' and 'C' stands for 'contact'. In this case, additionally to the use of brackets, the CLT plates are in direct contact and vibration transmission occurs through both plate-bracket and plate-plate interface (Fig. 2b);
– **C**, where 'C' stands for 'contact'. Here no bracket is employed to connect the plates. In this case, one CLT plate is resting perpendicular along the edge of

Table 1. Geometrical and mechanical properties of CLT100 and CLT060 plates. Parameters are defined referring to the Cartesian system of each plate, in which the z-axis is oriented along the plate thickness and the x-axis is oriented along the longer side of the plate.

Property	Units	Plate ID	
		CLT100	CLT060
Length	m	2.87	1.52
Width	m	..... 1.14	
Plies thickness	mm	[30/40/30]	[20/20/20]
Lay-up	°	[90/0/90]	[90/0/90]
Total thickness	mm	100	60
Density, ρ	kgm^{-3}	462	452
Loss factor, η	1	0.014	0.0083
Elastic moduli			
E_x	GPa	12.70	11.50
E_y	GPa	0.42	0.38
E_z	GPa	0.42	0.38
Poisson's ratios			
ν_{xy}	1	..... 0.10	
ν_{yz}	1	..... 0.30	
ν_{xz}	1	..... 0.10	
Shear moduli			
G_{xy}	GPa	0.79	0.72
G_{yz}	GPa	0.16	0.14
G_{xz}	GPa	0.79	0.72

the other, ensuring that vibration transmission occurs solely through the plates contact interface (Fig. 2c).

In configurations B and BC, the CLT plates were connected by two DX51D galvanized steel angle brackets, spaced 84 cm apart from their geometric centre, and fastened to the plates with eight steel screws, with a 40 mm thread length and 5 mm thread diameter. The global dimensions of the bracket are 90 (L) × 90 (H) × 65 (W) × 2.5 mm (T).

3.2 Modelling CLT plates

The two plates composing the L-junction mock-up are individually characterised, preliminarily to the simulation of the global CLT assembly. In particular, starting from the data obtained from experimental modal analyses conducted on both CLT plates in free boundary conditions, the FEM models of the plates were updated to retrieve the mechanical parameters of the material. Furthermore, to estimate the plates' loss factors, the experimental Power Injection Method (PIM) was applied [3]. The experimental setup and validation methodology employed for this purposes are analogous to that reported in [8, 9]. The plates' lay-ups and the elastic orthotropic parameters of the CLT plates are listed in Table 1.

The plates, numerically modelled in Ansys Mechanical (Release 2024, R2), are represented as orthotropic shells with 6 degrees of freedom, where the [90/0/90] orientation of the plies is modelled in a layer-wise representation.

Table 2. Comparison between the first eight numerical (f_k^{fe}, ϕ_k^{fe}) and experimental (f_l^{ex}, ϕ_l^{ex}) modes of the CLT100 plate in free-edge conditions.

Mode index	f_k^{fe} (Hz)	f_l^{ex} (Hz)	PE (%)	MAC (–)
(0,0)	20.1	19.9	0.6	0.99
(1,1)	38.8	38.7	0.1	1.00
(1,0)	54.8	54.2	1.2	0.99
(2,1)	80.2	80.1	0.1	0.99
(2,0)	106.1	103.0	2.9	0.98
(3,1)	126.9	127.4	0.4	0.98
(3,0)	172.6	169.3	1.9	0.85
(4,1)	181.6	182.1	0.3	0.93

Table 3. Comparison between the first eight numerical (f_k^{fe}, ϕ_k^{fe}) and experimental (f_l^{ex}, ϕ_l^{ex}) modes of the CLT060 plate in free-edge conditions.

Mode index	f_k^{fe} (Hz)	f_l^{ex} (Hz)	PE (%)	MAC (–)
(0,0)	35.1	35.8	1.9	1.00
(1,1)	43.6	42.0	3.6	1.00
(2,1)	93.8	90.3	3.7	0.99
(1,0)	96.0	96.8	0.8	1.00
(3,1)	158.7	153.3	3.4	0.99
(2,0)	185.6	187.4	1.0	0.98
(0,1)	216.9	213.9	1.4	0.87
(1,2)	230.6	224.7	2.6	0.88

Undamped FEM modal analyses are carried out separately on CLT100 and CLT060 standalone plates, in free edge conditions. Plates are discretised using quadratic triangular mesh, with a 4 cm maximum element size. The mesh elements, as defined above, are then utilised subsequently in the FEM model of the assembled L-junction, as depicted in Figure 1a.

The FEM models of the plates are validated against experimental data in the modal domain. Vibrometry tests were conducted on the same plates individually. Plate excitation was provided with an inertial shaker and normal velocities were measured with a Polytec PSV-400 laser Doppler vibrometer over a 17 × 7 point grid for the CLT100 plate and a 9 × 7 grid for the CLT060 plate. Measurement points were equally spaced approximately 18 cm apart. Plates were supported by inflated air jacks to replicate the free boundary conditions.

The validation is conducted by comparing the first eight numerical modes and related eigenfrequencies against those obtained from experimental measurements. The metrics utilised for validation are the MAC and PE indexes, defined in Section 2.3. The results of the validation are shown in Tables 2 and 3, where a good correlation in terms of MAC (above 0.85) and PE (below 5%) is observed for the first eight modes of the systems.

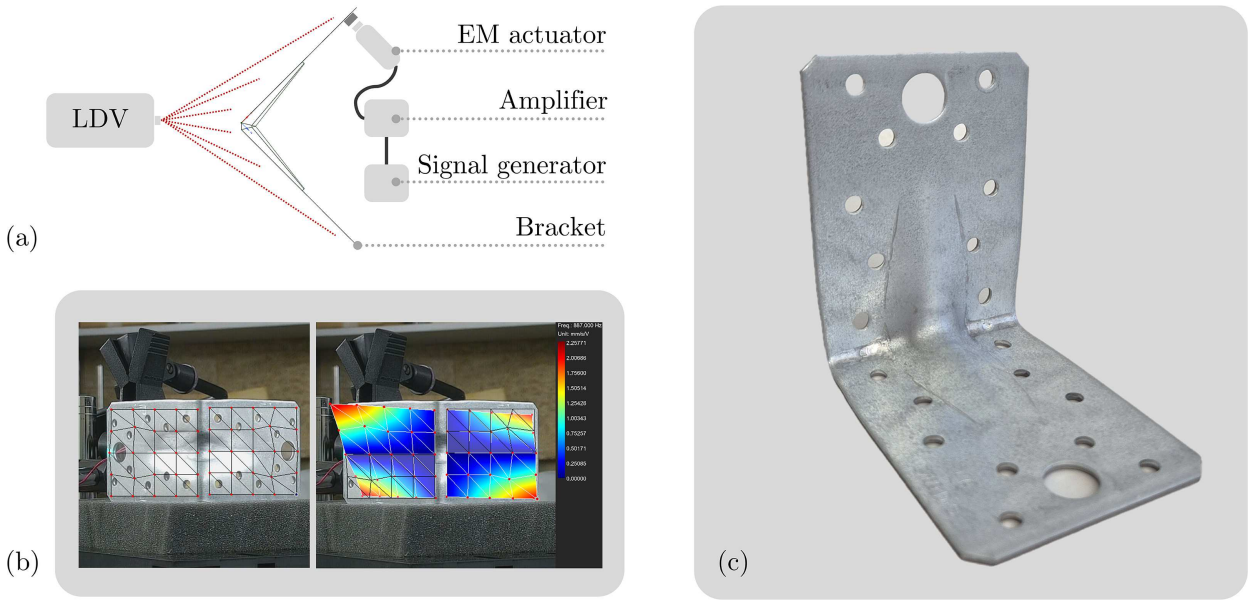

Figure 3. Experimental test set-up of a steel angle bracket: (a) Schematic of the measurement setup. (b) Measurement grid and velocity distribution acquired with a Laser Doppler Vibrometer. (c) Picture of the tested bracket sample.

3.3 Modelling connectors

The validation process of the detailed FEM model of a steel angle bracket is hereby outlined. The bracket model is described in Section 3.3.1 and the setup for laser Doppler vibrometry measurements is illustrated in Section 3.3.2. Numerical and experimental data are then compared for validation in Section 3.3.3.

3.3.1 Setup of the bracket FEM model

An angle bracket is numerically modelled in Ansys Mechanical (Release 2024, R2) and its geometry is reproduced in detail, starting from that of a commercially available galvanized steel bracket (Fig. 3c). It is modelled as an elastic isotropic shell element and discretised with 2 mm quadratic triangular mesh elements (Fig. 1d). For each node, three rotational and three translational degrees of freedom are defined. The modelling process is conducted by following progressive steps of geometry defeaturing, initially neglecting screw holes and gusset and then gradually refining the geometrical details, with regard to which the numerical model showed significant sensitivity. The optimal trade-off between efficiency and accuracy, shown in the Figure 1d, is validated according to the data reported in Section 3.3.3. Isotropic elasticity parameters for DX51D galvanized steel, drawn from [28], are defined as follows:

- Mass density, $\rho = 7830$ (kgm^{-3});
- Elastic modulus, $E = 210$ (GPa);
- Poisson's ratio, $\nu = 0.30$.

An undamped FEM modal analysis is performed, assuming the sample to have free boundary conditions.

3.3.2 Vibrometry measurements on a bracket

Vibration measurements on the steel angle bracket were carried out with an Optomet laser Doppler vibrometer. In order to ensure repeatability of the results, tests were performed on three different samples of the same bracket model. To replicate the free boundary conditions during measurements, brackets were resting on a layer of melamine foam. As visible in Figures 3a and 3b, mechanical excitation was applied at a corner position with an electromagnetic actuator to minimize possible effects on mass and stiffness of the sample. The actuator was driven by an amplified sine-sweep signal from the signal generator. The normal velocities were measured in an almost evenly spaced measurement grid with 13 mm point spacing (Fig. 3b). The frequency range was from 0 Hz to 6.4 kHz with a spectral resolution of 500 mHz. Ten measurements were averaged at each point and mobility was exported for every measurement point, in order to reconstruct the velocity distribution and to analyse the mobility response of the sample.

3.3.3 Bracket validation

The frequency response mobility functions L_Y, measured at a corner point of the three bracket samples is shown in Figure 4a together with their resulting average. Since only minor variation between the samples is observed by comparing such functions, it can be stated that measurements are repeatable and no relevant variation in the dynamical behaviour occurs among different samples of the same bracket. The natural frequencies of the bracket can be identified by the peaks of the mobility functions, showing that only nine modes occur within

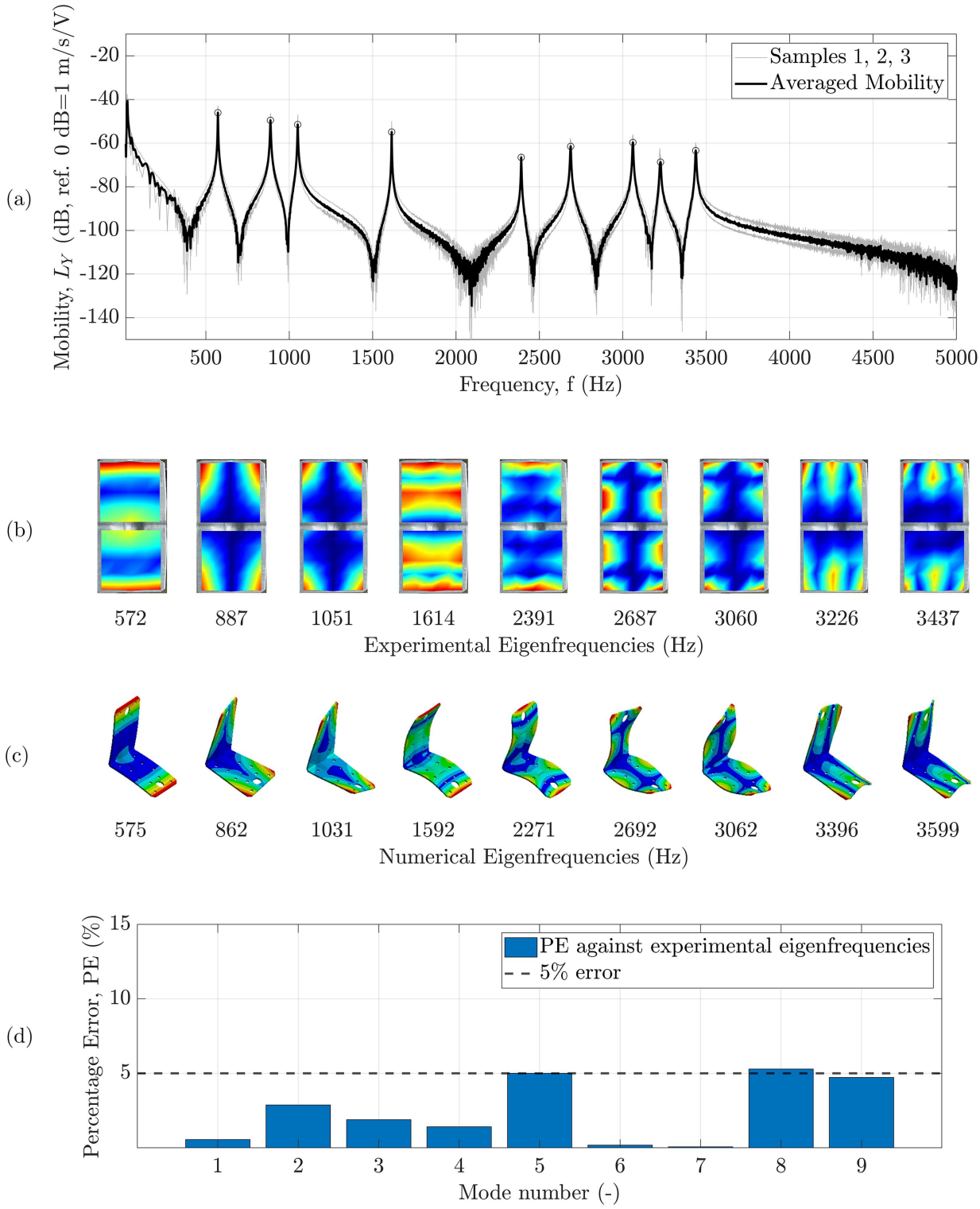

Figure 4. Validation of the FEM bracket model: (a) Point mobility response functions measured at a corner position of three samples of the same bracket model (in gray). The mobility function, averaged among the three samples, is represented in black. Abscissas of the circled peaks identify the eigenfrequencies of the bracket. (b) Measured mode shapes of the bracket and corresponding eigenfrequencies. (c) FEM mode shapes of the bracket and corresponding eigenfrequencies. (d) Percentage error between FEM and experimental eigenfrequencies.

the considered frequency range. At the corresponding frequencies, the measured mode shapes show a good agreement with the numerical results in the context of a qualitative comparison (Figs. 4b and 4c). With an observed PE of only up to 5.3% between numerical and experimental eigenfrequencies (Fig. 4d), the FEM model of the bracket can be considered as validated.

3.4 Modelling of interfaces

Following the characterisation and the validation of each single component of the L-junction (i.e. brackets and plates), physical connections at bracket-plate and plate-plate interfaces require a specific modelling approach. For both types of interface, Multi-Point Constraint (MPC) joints are defined, that introduce kinematic constraint equations to link displacements and rotations between the nodes of contacting elements, providing a linear solution and ensuring fast computation times [29].

Brackets are fastened to the plates by means of eight screws per bracket, as schematised in Figure 1d. To model the bracket-plate interface, the nodes along the edges of the bracket screw holes and the corresponding nodes projected onto the adjacent plates are linked and constrained to have the same solution as a single independent node located in a central position, at the origin of the joint reference system (Fig. 1d) [29]. In this case, no sliding, penetration or separation between the involved bodies is allowed.

The plate-plate interface case explicitly refers to configuration BC, where the CLT plates, connected by two brackets, are in direct contact with each other. Given the above, possible stiffening effects generated by the weight of the CLT060 plate standing on the CLT100 plate, have to be accounted for in view of numerical investigations on flanking sound transmission. In this case, bushing joints are defined, linking the degrees of freedom of node pairs selected along the common edge between the two plates. In particular, as highlighted with the red dots depicted in Figure 1e, each node of the pair is selected on the corresponding plate and numerically linked to the other with a stiffness coupling matrix. This matrix is populated with three translational and three rotational stiffness coefficients for the x, y and z axis directions. To model the direct contact between plates in configuration BC, values of 1×10^{10} N/m and 1×10^{10} N·m/rad are respectively assigned to the translational and rotational stiffness coefficients, in order to approach to rigid contact conditions. For the modelled CLT L-junction, node pairs are defined with an approximate spacing of 4 cm, in order to comply, where possible, with the maximum mesh element size. Modelling the line contact with coupling stiffness matrices potentially adds greater versatility to the model.

3.5 Modelling the L-junction

Undamped modal analyses and damped forced response analyses are conducted in FEM for the L-junction system in free-edge conditions, using the Ansys Mechanical (Release 2024, R2) software. For the harmonic analyses, the frequency-independent plates' structural loss factors, reported in Table 1, are included in the model. As a result of the modal analyses, eigenfrequencies and mode shapes of the first sixteen modes are used for calculating PE and MAC indexes against experimental data for validation in the low modal density region. More details about the validation process will be discussed in Section 4. As an output of the harmonic analyses, plate normal surface velocities are mapped using two dimensional linear interpolation to the grid points used for laser vibrometer measurements. The measurement point grids for CLT100 and CLT060 plates are the same as those defined in Section 3.2 for measurements on decoupled plates. Mechanical excitation is provided by sequentially applying harmonic forces of 1 N amplitude at the points F_1 to F_6, as highlighted in Figure 1a. For each excitation point, plate average velocity levels were computed to calculate the direction-averaged level difference $\overline{D_{v,ij}}$. A logarithmic solution interval was defined for the full harmonic analysis, ranging from 178 Hz to 3548 Hz with 657 frequency steps. To calculate the equivalent absorption lengths $a_{i,j}$ of the plates according to equation (6), the structural reverberation time $T_{s,i,j}$ of the ith and jth plates in coupled conditions is evaluated in one third-octave bands. For this purpose, the PIM is applied to the numerical results to calculate the loss factor $\eta_{i,j}$ of the coupled plates. According to [3], $T_{s,i,j}$ was calculated as:

$$T_{s,i,j} = \frac{2.2}{f\ \eta_{i,j}} \tag{10}$$

where f represents the center frequency of the one third-octave band of interest. To present an overview of the damping provided by the experimental setup and the different connector configurations, the measured structural reverberation times of plates CLT100 and CLT060 in coupled conditions are reported in Figure 5 for each configuration of the L-junction. As for the numerical data, these results were obtained by applying PIM to the measured data. Results of the validation in the mid-to-high frequency range, in terms of K_{ij}, are provided in Sections 4.2.1 and 4.2.2.

4 Validation of the L-junction model against experiment

In this section, the validation process of the L-junction model is outlined. The setup for vibrometry measurements is described in Section 4.1. In Section 4.2, a comparison is shown between numerical results and the experimental data measured on configurations B and BC of the test set-up, for validation both at low frequency (in terms of MAC and PE) and in the high modal density region (in terms of K_{ij}). Measured data from configuration C are not considered for the purpose of model validation. These data are reported exclusively to support the analysis in Section 5.1, where the effects of connectors and

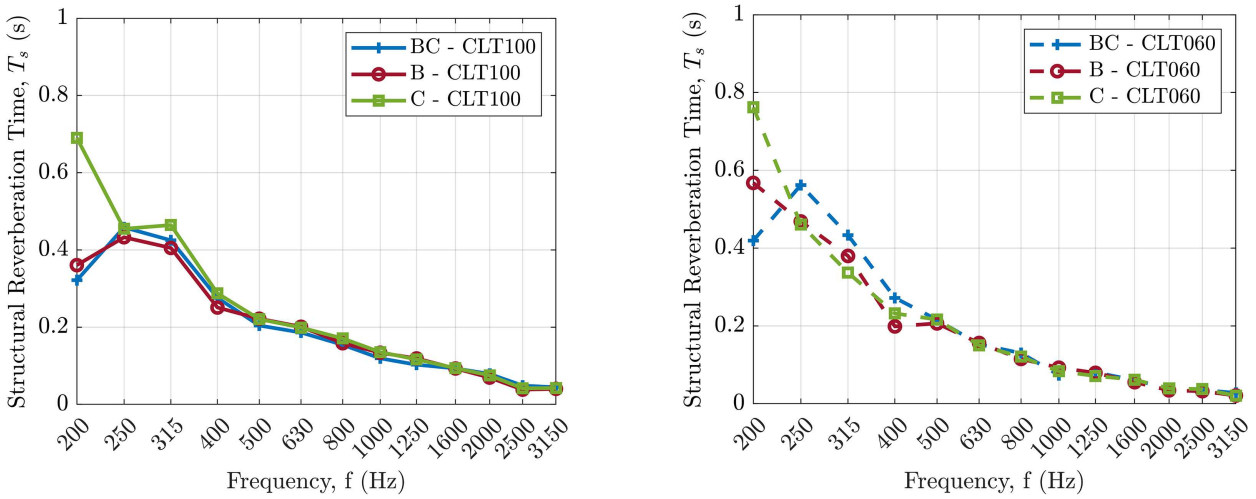

Figure 5. Measured structural reverberation times of CLT plates in coupled conditions for B, BC, and C configurations: (a) plate CLT100; (b) plate CLT060. Data are reported in one-third octave bands.

plate-to-plate contact on flanking sound transmission are investigated experimentally. The deterministic definition of coupling stiffness coefficients to simulate the mechanical contact at the plate-plate interface in absence of connectors would have required the application of further modelling strategies that are out of the scope of this work.

4.1 Experimental setup

An L-junction mock-up with the same dimensions of the model described in Section 3 was built for the purpose of vibrometry measurements in the lightweight building facility at Empa. The three different configurations of the mock-up, introduced in Section 3.1, were tested (Fig. 2). In order to experimentally achieve free boundary conditions and isolate the samples from possible sources of vibration transmitting through the ground, the tested specimens were resting on four air-jacks. These were located close to the corners of the CLT100 plate, and their internal air pressure has been kept constant during the measurements. For configurations B and C, a wooden frame supporting the sample was built for safety reasons, preventing possible tipping or slipping of the vertical plate (Fig. 2a and 2c). In particular, the vertical CLT plate was isolated from the frame structure by interposing air jacks and/or layers of resilient foam. According to the ISO 10848-1:2017 standard [23], the plates' normal velocities were acquired and then post-processed for the calculation of K_{ij} indexes. It should be noted that there were some deviations from the standard due to the scaled size of the test specimen. This implied that the assumption of the modal overlap factor $M > 1$ above 250 Hz was not met. This quantity reached unity between the 500 Hz and 630 Hz one-third octave-bands for configuration BC. Furthermore, due to the free-edge boundary conditions of the sample, the distance criteria for the excitation and measurement positions were not adhered to. Moreover, data were measured over an evenly spaced point grid using a Polytec PSV-400 scanning head, which ensured a high spatial resolution of measured data, necessary for comparing experimental and numerical mode shapes. The measurement point grids for CLT100 and CLT060 plates were the same as those defined in the FEM model setup. The acquisition was conducted over a frequency range from 0.06 Hz to 5656 Hz with a frequency spacing of 62.5 mHz and complex averaged over five measurements for each point. As defined in the numerical model and shown in Figure 1a, three excitation points per plate were chosen, one close to a corner (F_1 and F_4) and the other two in proximity at the midpoint of the plate sides (F_2, F_3 and F_5, F_6). In configuration BC, mechanical excitation was provided by means of a Data Physics IV40 inertial shaker, driven by a swept sine test signal. In configurations B and C, a Brüel & Kjær 4809 shaker was used to increase the amount of vibrational energy injected into the sample at high frequency. This was necessary as less power was transmitted at the connection due to the reduced coupling of the plates. In both cases, shakers were linked to a signal amplifier, connected to the Polytec PSV-400 laser vibrometer system (Fig. 6). Reference signals, namely force and acceleration at the excitation point, were measured with a PCB impedance head, mounted between the shaker and the test sample.

4.2 Results and validation

In this subsection, the numerical results from modal and harmonic analyses are compared to experimental data obtained from the vibrometry measurements performed on configurations B and BC. Configuration C was tested only experimentally and not simulated in FEM, since the definition of nodal stiffness coupling coefficients

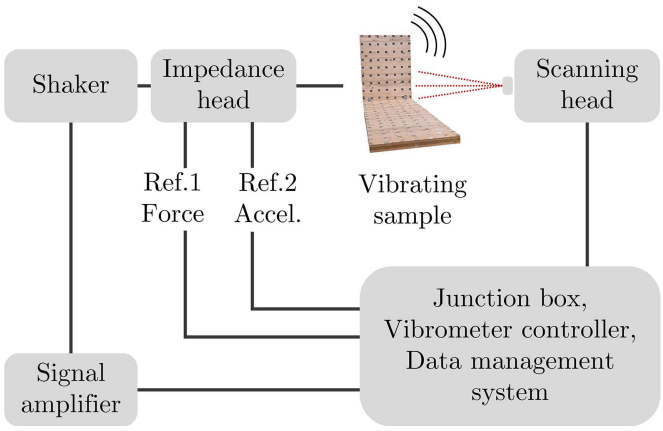

Figure 6. Schematisation of the Polytec PSV-400 laser Doppler vibrometer measurement chain.

would have required the application of model updating algorithms which are out of the scope of this paper. The FEM model is validated both in the low and high modal density regions. In the first case, this is done by computing the MAC and PE indexes against the experimental data for the first sixteen modes of the system, up to 200 Hz. Further details on the results of the experimental modal analysis conducted on both the L-junction configurations can be found in [30]. From 200 Hz to 3150 Hz, due to the increased modal density of the system, data are compared in terms of the K_{ij} index.

4.2.1 Configuration B

This configuration is set to ensure that vibrations are propagating only through the steel brackets, with no flanking transmission occurring at the plate-plate contact interface. Consequently, brackets are modelled numerically and constrained to the CLT plates with MPC joints. Coupling stiffness coefficients at node pairs along the contact edge between plates are neglected for this configuration. To validate the model in the low modal density region, the first sixteen eigenmodes are considered for comparison against experimental data. In particular, for each mode, the PE and MAC indexes are calculated, as defined in equations (8) and (9). As visible in Table 4, the percentage error against experimental eigenfrequencies is at most equal to 5.6%, with an average value of 3.6%, excluding the first eigenmode. For this mode, occurring at 2.8 Hz, a 30.8% PE and a 0.73 MAC values are observed against experimental results. This specific eigenmode corresponds to the first global resonance of the system, where none of the two CLT plates are undergoing significant flexural or torsional deformation, but are rotating around the common edge axis. Since this resonance occurs at very low frequency, the absolute value difference between eigenfrequencies provides a more realistic assessment of the actual deviation from experimental data at this eigenmode, which is found to be equal to 0.7 Hz. For higher order modes, MAC matrix diagonal values are at least equal to 0.70. Above 200 Hz, the comparison between numerical and measured K_{ij} is presented in one third-octave frequency bands up to 3150 Hz, as shown in Figure 7a. Alongside the FEM and experimental K_{ij} curves, the absolute value difference $|\Delta K_{ij,\mathrm{FEM-Exp}}|$ between FEM and experimental results is plotted in a bar graph. As observable, a good correlation is achieved between FEM and measured data, with an average deviation of 1.5 dB and a maximum deviation of 3.6 dB, occurring at the 1 kHz third-octave band. Single-number K_{ij} averaged over the mid-frequency (250 Hz–1 kHz) and high-frequency (1.25 kHz–3.15 kHz) ranges were calculated, as defined in the ISO 10848-1:2017 standard [23]. The deviations between the numerical and experimental single-number ratings are found to be equal to 1.4 dB for the $\overline{K_{ij,\mathrm{mid}}}$ index and to 0.9 dB for the $\overline{K_{ij,\mathrm{high}}}$ index. These results clearly demonstrate that vibration and structure-borne sound transmission at an L-junction can be modelled accurately by simplifying fasteners with MPC rigid joints.

Table 4. Comparison between the first eight numerical (f_k^{fe}, ϕ_k^{fe}) and experimental (f_l^{ex}, ϕ_l^{ex}) modes of configuration B.

Mode number	f_k^{fe}(Hz)	f_l^{ex}(Hz)	PE (%)	MAC (–)
1	2.1	2.8	30.8	0.73
2	16.5	16.3	0.9	0.75
3	20.5	19.6	4.4	0.88
4	23.8	24.0	0.8	0.70
5	25.5	24.3	4.8	0.88
6	48.6	47.2	2.8	0.86
7	60.3	58.9	2.4	0.87
8	69.7	66.4	4.7	0.93
9	77.4	73.5	5.1	0.95
10	97.8	93.7	4.2	0.83
11	106.5	104.0	2.3	0.87
12	129.9	124.0	4.5	0.94
13	148.8	140.4	5.6	0.87
14	161.6	154.4	4.5	0.80
15	164.6	161.6	1.8	0.82
16	206.9	196.3	5.1	0.80

4.2.2 Configuration BC

In this configuration, CLT plates are connected with brackets and, additionally, they are in direct contact with each other along their common edge. Thus, in addition to the brackets, modelled as in configuration B, stiffness coupling matrices are introduced to model the surface contact at the node pairs along the common edge between the plates. To approximate rigid contact conditions, the six translational and rotational stiffness entries are defined to be respectively equal to 1×10^{10} N/m and 1×10^{10} N·m/rad. To validate the model in the low modal density region, PE and MAC indexes between the FEM model and experimental measurements are reported in Table 5. Also in this case, the highest deviation in terms of PE is observable at the first eigenmode (45.6%), with

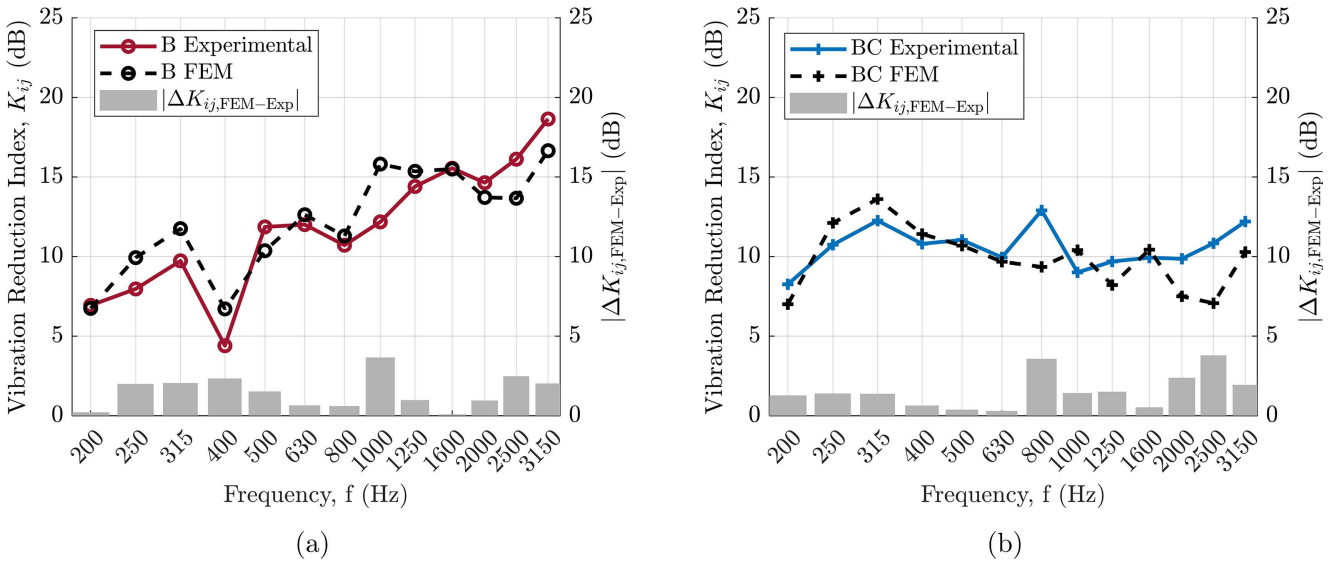

Figure 7. Comparison between numerical and experimental K_{ij}: (a) configuration B; (b) configuration BC.

Table 5. Comparison between the first eight numerical (f_k^{fe}, ϕ_k^{fe}) and experimental (f_l^{ex}, ϕ_l^{ex}) modes of configuration BC.

Mode number	f_k^{fe} (Hz)	f_l^{ex} (Hz)	PE (%)	MAC (–)
1	5.6	3.0	45.6	0.74
2	17.0	17.0	0.1	0.74
3	22.0	21.2	3.4	0.72
4	24.8	24.6	1.2	0.71
5	32.9	28.2	14.3	0.92
6	50.4	48.8	3.2	0.83
7	61.4	62.4	1.6	0.91
8	75.5	70.2	7.0	0.96
9	87.5	80.2	8.3	0.83
10	103.8	96.6	6.9	0.69
11	107.7	108.9	1.1	0.91
12	139.4	131.0	6.1	0.94
13	158.3	155.9	1.6	0.81
14	163.5	162.3	0.8	0.82
15	183.2	166.9	8.9	0.81
16	217.8	213.3	2.1	0.86

an absolute value of the deviation between FEM and measured eigenfrequencies of 2.6 Hz and a MAC value of 0.74. For the remaining fifteen modes, the average PE value is found to be equal to 4.4%, with a peak value of 14.3% occurring at the fifth mode, where the correlation with a MAC of 0.92 is nevertheless very high. On the other hand, the lowest MAC value (0.69) is observed at the 10th mode, where the percentage error between the corresponding eigenfrequencies is 6.9%. At higher frequencies, the comparison in terms of K_{ij}, is observable in Figure 7b. In this case, the average deviation $\left|\Delta K_{ij,\mathrm{FEM-Exp}}\right|$ is equal to 1.5 dB, with a maximum value of 3.8 dB at the 2500 Hz one third-octave band. Deviations in terms of $\overline{K_{ij,\mathrm{mid}}}$ and $\overline{K_{ij,\mathrm{high}}}$ are found to be, respectively, 0.1 dB and 1.8 dB.

5 Discussion and further analyses

In Section 5.1, the effects of connectors as well as mechanical contact between plates on the flanking transmission in CLT junctions are further analysed. In Section 5.2, further discussion is given to evaluate the scope of applicability and the limitations of the presented methodology.

5.1 Effects of connectors and plates' contact on flanking sound transmission

In this subsection, the effects of the mechanical contact between plates as well as the influence of connectors in CLT L-junctions are investigated by analysing the experimental K_{ij} trends measured on the three sample configurations defined in Section 3.1.

In particular, in Figure 8a, the K_{ij} indexes of configurations BC and B are compared. It can be observed that, across the range of low to high frequencies, the sign of the difference between the two curves undergoes a reversal, with the exception of a region that occurs at medium frequency, where the two curves exhibit similar values. In particular, in the frequency range from 500 Hz to 800 Hz, the K_{ij} curves are in close proximity to one another, with a maximum difference of 2.2 dB. This range might be interpreted as a cross-over region below and above which the two systems exhibit different behaviour. In particular, from 200 Hz to 400 Hz, the two K_{ij} curves demonstrate an average absolute difference value of 3.3 dB, with the BC showing higher K_{ij} values in all bands. This implies some considerations on the modal overlap factor of the system, as defined in equation (7). For configuration BC,

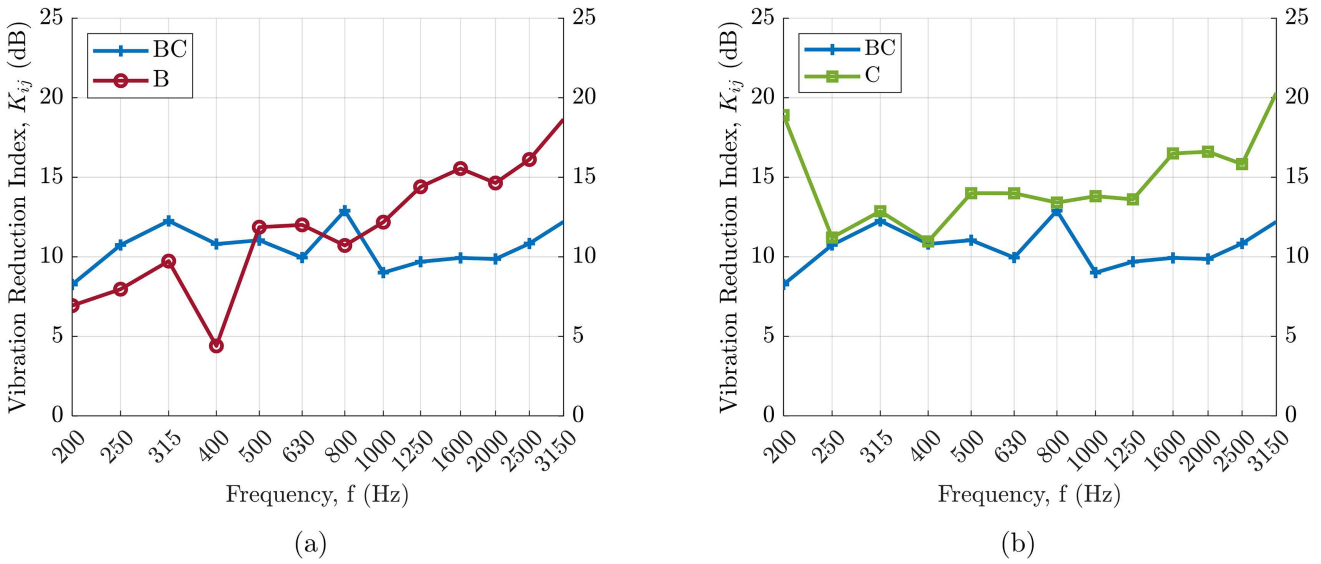

Figure 8. Comparison of experimental K_{ij} between sample configurations: (a) BC vs. B; (b) BC vs. C.

this parameter reaches a value of 1 between the 500 Hz and 630 Hz one third-octave bands. For this reason, K_{ij} data below 630 Hz are subject to possible over- or underestimation and therefore any conclusion regarding the dynamics of the sample in this frequency range should refer to alternative and more reliable indicators. Conversely, above 630 Hz, it is evident how the amount of energy transmitted through the junction in configuration B is lower than in the BC case, due to the plates being decoupled by an air gap. Indeed, in this range, the K_{ij} of configuration B is on average 4.3 dB greater of that from configuration BC, and a deviation of 5.4 dB is observable in terms of $\overline{K_{ij,\text{high}}}$ between the two configurations. This shows that the use of connectors in conjunction with the mechanical contact between plates significantly increases flanking transmission in the high modal density region.

To investigate the effects of connectors at the CLT plates' interface, K_{ij} from configurations BC and C are compared in Figure 8b. Also in this case, the discussion is restricted to the frequency range above 630 Hz, where the modal overlap factor of configuration BC exceeds unity. In this range, the two curves start to significantly diverge and a 5 dB average deviation is observable, with a difference in terms of $\overline{K_{ij,\text{high}}}$ of 6.1 dB. In particular, the K_{ij} of configuration C is consistently higher, confirming that, for this specific case, the use of connectors contributes to increase flanking transmission. This analysis suggests that the simultaneous application of connectors and plate contact has a greater stiffening effect than applying only one of the constraint conditions. Nevertheless, this statement is not universally valid and is subject to further investigation, possibly involving experimental tests on heavier systems. Indeed, it is worth to note that, for the specific case in question, friction or pre-loading effects due to the surface contact are exclusively attributable to the gravity load of the CLT060 plate which, in configuration BC and C, is vertically resting onto the CLT100 plate. A possible further decrease of K_{ij} at high frequency, due to heavier loads applied vertically on the L-junction, i.e. typical operational loads in CLT buildings, constitutes a point of further experimental research. This may be useful also to investigate whether a trend in the variation of the stiffness coefficients in the coupling matrices can be outlined as the mechanical load on the connection varies. Based on the above analyses, it can be stated that an interrelationship exists between fasteners and contact mechanics at the plate interface. Nevertheless, no explicit relationship has been derived yet.

5.2 Limitations and applicability of the method

In this subsection, limitations and possible extensions of the proposed predictive methodology are discussed. For this purpose, the K_{ij} data, already shown in Figure 7, are further compared in Figures 9c and 10c to the numerical results obtained from additional simplified FEM models of configurations BC and B.

In particular, for configuration BC, the numerical model depicted in Figure 9a is simplified to a rigid line connection. Hereby, the brackets are suppressed applying the nodal stiffness coupling coefficients, already used to simulate the contact at the plate-plate interface, to the node pairs along the entire edge between the plates (Fig. 9b), holding an approximate spacing of 4 cm. This way, the necessity of modelling connectors in detail is investigated for the specific case in question. As shown from the bar graph in Figure 9c, the maximum absolute difference value $\left|\Delta K_{ij,\text{FEM,simpl}-\text{FEM}}\right|$ between the original and simplified FEM models of configuration BC is found to be equal to 1.4 dB. Upon initial observation of the presented case, involving contact and fasteners, the connection behaves as a rigid line interface. This suggests that modelling connectors in detail would be redundant and that rigid line connections would be sufficient

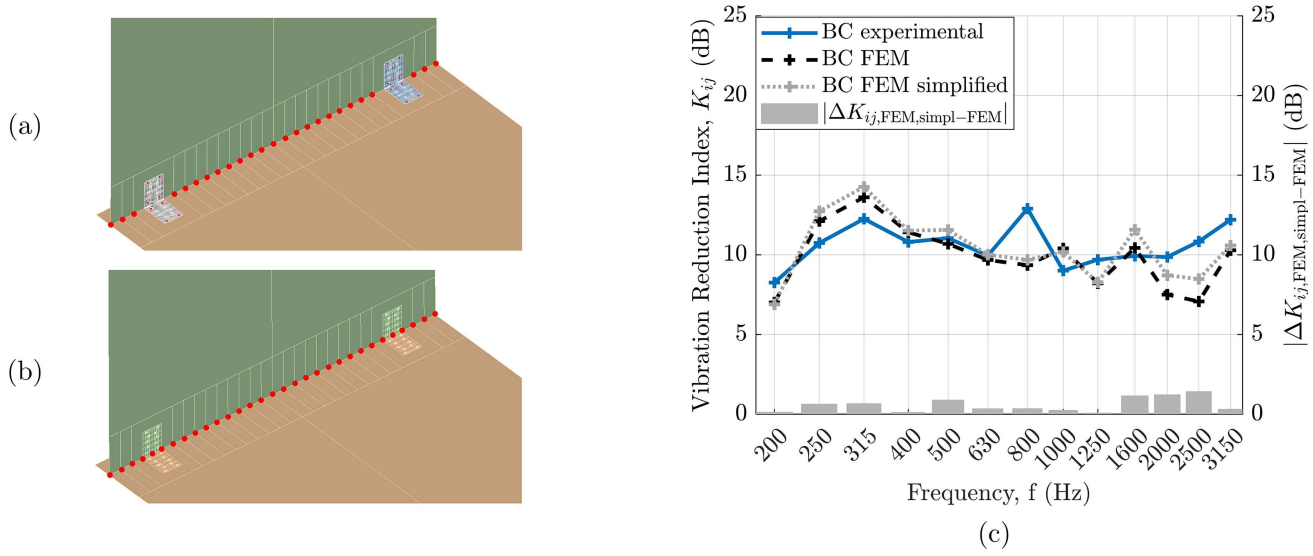

Figure 9. Configuration BC: (a) Schematisation of the MPC joints for bracket fastening and plate-plate contact interface in the original 'BC FEM' model. (b) Schematisation of the MPC joints for plate-plate contact interface in the 'BC FEM simplified' model. (c) Comparison between the experimental and the numerical K_{ij} from the original FEM model (BC FEM) and the simplified FEM model (BC FEM simplified).

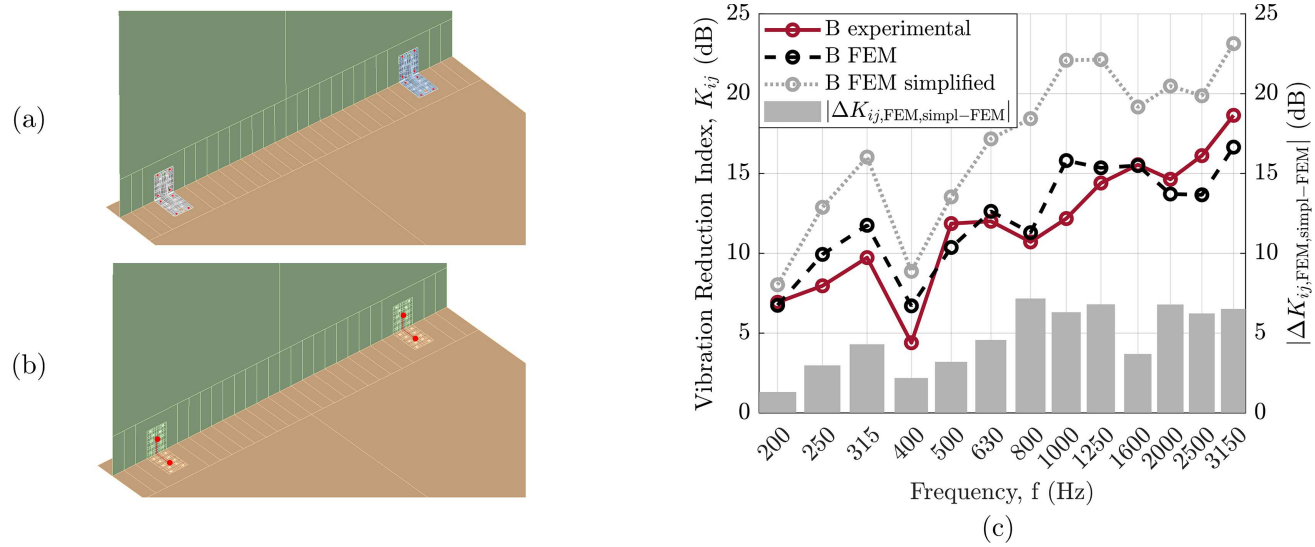

Figure 10. Configuration B: (a) Schematisation of the MPC joints for bracket fastening in the original 'B FEM' model. (b) Schematisation of the nodal stiffness joints, used to replace brackets in the 'B FEM simplified' model. (c) Comparison between the experimental and the numerical K_{ij} from the original FEM model (B FEM) and the simplified FEM model (B FEM simplified).

to model this type of junctions. Nevertheless, it is likely that, for the specific case in question, the analysed sample might demonstrate a high level of similarity with the behaviour of a rigid junction, due to the mechanical and geometrical properties of the plates as well as the brackets' spacing.

With the aim of investigating possible applications of this methodology to cases where the contact interface between plates is far from rigid, the experimental and numerical data presented in Figure 10c can be taken as a reference. In this case, the effects of a simplification in the bracket model are investigated. In particular, starting from the original FEM model of configuration B (in Fig. 10a), connectors are simplified by linking two nodes lying approximately at the center of each bracket footprint onto the CLT plates, as depicted in Figure 10b. These nodes are connected with coupling stiffness matrices, the entries of which are 1×10^{10} N/m for the translational stiffnesses and 1×10^{10} N·m/rad for the rotational stiffnesses. As visible from the plot in Figure 10c, the absolute difference value between the original and the simplified FEM models, is considerably higher than in the BC case. In particular, the average deviation is found to be 4.7 dB with a maximum value of 7.1 dB. This suggests

that, for the case in question, modelling the connectors in detail provides a considerably higher accuracy and that, at this stage, fasteners cannot be simplified to mere rigid point connections. Nevertheless, this does not exclude the possibility of reducing the model order of the brackets to an elastic point connection. However, to achieve reliable reduction strategies, an appropriate dynamic characterisation of the connectors is necessary, implying preliminary numerical modelling and experimental validation of the connectors, as described in Section 3.3.

Some of the findings of the authors' previous research work conducted at Empa can further motivate the necessity of modelling connectors in detail. In [15], a mass timber T-junction with an elastic interlayer at the interface of the plates was parametrically investigated, with the aim of determining the improvement achieved, in terms of K_{ij}, with respect to a reference junction case. In the latter, plates were connected with steel angle brackets and no elastic interlayer was used for decoupling plates. Three different configurations of the T-junction were tested: the first one, where no bracket was utilised to connect plates; a second configuration, where three steel angle brackets, decoupled from the plates with an elastic interlayer, were utilised to connect the plates; a third configuration, where the brackets were rigidly fastened to the plates without any decoupling layer. The K_{ij} improvement of each configuration with respect to the reference case is hereby analysed relatively to the corner transmission path along the upper vertical and the horizontal plate. It is observed that a substantial K_{ij} increase was achieved in the case of the decoupled brackets, whilst in the case of the rigidly applied brackets the K_{ij} improvement was significantly smaller. This is also confirmed by observing that the $\overline{K_{ij,\mathrm{mid}}}$ of the sample with decoupled brackets was 6.7 dB greater than that with rigid brackets. The motivation for this further experimental investigation lies in the fact that, assuming to be able to model the interface between plates with an interposed elastic layer by using linear springs, it is clear that a detailed model of the connectors becomes crucial to obtain accurate predictions, especially when they are elastically decoupled from the CLT plates. In this latter case, possible modelling approaches might aim to define coupling stiffness coefficients to represent the fastening strength at the plate-bracket interface, considering the additional mechanical effects due to the presence of an interposed elastic layer. Nevertheless, this issue is to be considered an open research question for the purposes of further investigation in this field.

6 Conclusions

This paper presents a numerical approach for the calculation of flanking sound transmission in CLT L-junctions. Alongside the existing predictive models, mostly built upon simplifications of the connections, the proposed methodology emphasises the effectiveness of modelling connectors in detail, providing a dynamic characterisation of CLT junction components. This may constitute the preliminary stage of a bottom-up procedure for building broadband versatile FEM models, which could possibly account for the effects of a change in the number and position of connectors in the junction. This latter point is currently under investigation.

The methodology is based on the use of FEM for modelling a CLT L-junction mock-up, which is validated not only in the low modal density range but also at higher frequencies, by calculating K_{ij} up to 3150 Hz. Plates are modelled as shells and the detailed geometry of angle brackets is included in the model. The modal dynamics of metal angle brackets is investigated, by validating a FEM model of a commercially available sample against experimental measurements. This is then integrated into the FEM model of an assembled L-junction mock-up, where simplifications are adopted for modelling both bracket fastening and the mechanical contact at the plate-plate interface.

With reference to the former point, validation against experimental data has shown that the numerical representation of fastening with rigid multi-point constraints is applicable to the case under discussion.

The mechanical contact at plates interface is modelled by linking node pairs at the edge of the connected plates by means of coupling stiffness matrices. The utilised stiffness values approach the behaviour of a rigid connection which, according to the evidence provided by experimental data, is applicable to the case in question. Nevertheless, the derivation of such coefficients depends on the specific build-up conditions of the analysed sample, such as the number and type of connectors and possible preloading conditions of the junctions, as is typical for the case of in-situ conditions, due to the weight of ceilings or upper story walls.

Additional numerical investigations have shown that detailed bracket models predicted structure-borne sound transmission better than simplified rigid point connections. Nevertheless, this does not exclude the possibility of simplifying the connectors with nodal coupling matrices, although this implies an accurate dynamic characterisation of the connectors prior to the application of model order reduction strategies.

The experimental investigation, based on the comparison of the three sample configurations, has shown that the vibration reduction index is influenced by both plate contact and connectors. In particular, for the specific case in question, none of the two constraint conditions is dominant with respect to the other. On the other hand, it is evident that a correlation exists between connectors and contact mechanics at the plate interface. The derivation of an explicit relationship to describe this interaction represents a potential subject for further research.

Acknowledgments

The authors would like to thank Nino Blumer for his assistance with the experimental set-up and Liviu Zambila for his insights on FEM simulations.

Funding

The authors gratefully acknowledge the financial support of the research project by the Swiss Federal Office for the Environment as part of the Aktionsplan Holz.

Conflicts of interest

The authors declare no conflicts of interest.

Data availability statement

Data are available on request from the authors.

References

1. J.M. Greene, H.R. Hosanna, B. Willson, J.C. Quinn: Whole life embodied emissions and net-zero emissions potential for a mid-rise office building constructed with mass timber. Sustainable Materials and Technologies 35 (2023) e00528.
2. R. Azari, M. Singery: Laminated timber buildings: an overview of environmental impacts, in: A. Sayigh, Ed. The Importance of Wood and Timber in Sustainable Buildings. Springer, Cham, Switzerland, 2022.
3. L. Cremer, M. Heckl: Structure-Borne Sound: Structural Vibrations and Sound Radiation at Audio Frequencies. Springer, Berlin, Heidelberg, Germany, 2005.
4. S. Zoellig, M. Muster, A. Themessl: Butt-joint bonding of timber as a key technology for point-supported, biaxial load bearing flat slabs made of cross-laminated timber, in: Proceedings of Sustainable Built Environment D-A-CH Conference 2019, Graz, Austria. IOP Conference Series: Earth and Environmental Science. Vol. 323, 2019, 012144 pp.
5. S. Zhang, Y.H. Chui: Characterizing flexural behaviour of panel-to-panel connections in cross-laminated timber floor systems. Structures 28 (2020) 2047–2055.
6. F. Morandi, S. De Cesaris, M. Garai, L. Barbaresi: Measurement of flanking transmission for the characterisation and classification of cross laminated timber junctions. Applied Acoustics 141 (2018) 213–222.
7. Z. Li, K.D. Tsavdaridis: Design for seismic resilient cross laminated timber (CLT) structures: a review of research, novel connections, challenges and opportunities. Buildings 13, 2 (2023) 505.
8. S. Vallely, S. Schoenwald: An efficient analytical method to obtain the homogenised frequency-independent elastic material properties of cross-laminated timber elements. Journal of Sound and Vibration 546 (2023) 117424.
9. S. Vallely, S. Schoenwald: Higher-order modal parameter estimation and verification of cross-laminated timber plates for structural-acoustic analyses. Acta Acustica 8 (2024) 52.
10. ISO 12354-1:2017: Building acoustics – Estimation of acoustic performance of buildings from the performance of elements – Part 1: airborne sound insulation between rooms, standard, International Organization for Standardization, Geneva, CH, 2017.
11. C. Guigou Carter, M. Villot: Junction characteristics for predicting acoustic performance of lightweight wood-based buildings, in: Proceedings of Internoise 2015, San Francisco, CA, 2015.
12. C. Guigou Carter, N. Balanant, J.L. Kouyoumji: Acoustic performance investigation of a CLT-based three-floor building. Buildings 13, 8 (2023) 1935.
13. S. Moons, R. Lanoye, E.P. Reynders: Prediction of flanking sound transmission through cross laminated timber junctions with resilient interlayers. Applied Acoustics 228 (2025) 110317.
14. R. Langley, K. Heron: Elastic wave transmission through plate/beam junctions. Journal of Sound and Vibration 143, 2 (1990) 241–253.
15. S. Schoenwald, N. Kumer, S. Wiederin, N. Bleicher, B. Furrer: Application of elastic interlayers at junctions in massive timber buildings, in: Proceedings of International Congress on Acoustics, Aachen, Germany, 2019.
16. M. Izzi, A. Polastri, M. Fragiacomo: Modelling the mechanical behaviour of typical wall-to-floor connection systems for cross-laminated timber structures. Engineering Structures 162 (2018) 270–282.
17. M. Salvalaggio, F. Lorenzoni, M.R. Valluzzi: Impact of sound-insulated joints in the dynamic behavior of cross-laminated timber structures. Journal of Building Engineering 91 (2024) 109525.
18. M. Fragiacomo, B. Dujic, I. Sustersic: Elastic and ductile design of multi-storey crosslam massive wooden buildings under seismic actions. Engineering Structures 33, 11 (2011) 3043–3053.
19. J.A. Steel, R.J.M. Craig: Statistical energy analysis of structure-borne sound transmission by finite element methods. Journal of Sound and Vibration 178, 4 (1994) 553–561.
20. C. Hopkins: Vibration transmission between coupled plates using finite element methods and statistical energy analysis. Part 1: comparison of measured and predicted data for masonry walls with and without apertures. Applied Acoustics 64, 10 (2003) 955–973.
21. C. Hopkins, C. Crispin, J. Poblet-Puig, C. Guigou-Carter: Regression curves for vibration transmission across junctions of heavyweight walls and floors based on finite element methods and wave theory. Applied Acoustics 113 (2016) 7–21.
22. A. Esposito, S. Vallely, S. Schoenwald: Modelling cross-laminated timber plate connections: a numerical investigation on flanking sound transmission through angle brackets, in: Proceedings of Forum Acusticum Euronoise 2025, Málaga, Spain, 2025.
23. ISO 10848-1:2017: Acoustics – Laboratory and field measurement of flanking transmission for airborne, impact and building service equipment sound between adjoining rooms – Part 1: frame document, International Organization for Standardization, Geneva, CH, 2017.
24. ISO 10848-4:2017: Acoustics – Laboratory and field measurement of flanking transmission for airborne, impact and building service equipment sound between adjoining rooms – Part 4: application to junctions with at least one Type A element, International Organization for Standardization, Geneva, CH, 2017.
25. S.V. Modak: Analytical and Experimental Modal Analysis. CRC Press Taylor & Francis Group, Boca Raton, USA, 2023.
26. Ansys® Academic Research Mechanical APDL 2024: Release 24.2, Help System, Theory Reference, ANSYS, Inc.
27. R.J. Allemang: The modal assurance criterion – Twenty years of use and abuse. Sound and Vibration 37, 8 (2003) 14–23.
28. R. Vasile, S.G. Racz, O. Bologa: Experimental and numerical investigations of the steel sheets formability with

hydroforming, in: Proceedings of MATEC Web of Conferences CoSME'16, 02016, 2017.
29. Ansys® Academic Research Mechanical APDL 2024: Release 24.2, Help System, Mechanical User's Guide, ANSYS, Inc.
30. S. Vallely, A. Esposito, S. Schoenwald: Experimental modal analysis of a cross-laminated timber L-junction with a view towards predicting flanking sound transmission, in: Proceedings of Forum Acusticum Euronoise 2025, Málaga, Spain, 2025.

Cite this article as: Esposito A. Vallely S. Kurent B. & Schoenwald S. 2026. Finite element modelling of bracket-connected cross-laminated timber plates to calculate vibration reduction indices. Acta Acustica, **10**, 39. https://doi.org/10.1051/aacus/2026036.